Energy and Buildings 43 (2011) 1139–1148

Contents lists available at ScienceDirect

Energy and Buildings

journal homepage: www.elsevier.com/locate/enbuild

Thermal conditions and ventilation in an ideal city model of Hong Kong

Lina Yang*, Yuguo Li

Department of Mechanical Engineering, The University of Hong Kong, Pokfulam Road, Hong Kong, China

ARTICLE INFO

Keywords:
Urban thermal environment
Thermal buoyancy
Thermal stratification
City ventilation

ABSTRACT

Urban heat island can significantly increase the demand for cooling of buildings in cities. This paper investigates one of the main causes of the urban heat island phenomenon, i.e. reduced city ventilation. Two simple Hong Kong city models with relatively complex terrain were considered here under different atmospheric conditions. A 3D RNG k–ε turbulence model was used for modeling turbulence effects. The simulation results showed that the influence of thermal stratification can be significant on city ventilation driven partially by thermal buoyancy. When the wind speed is relatively large, the impact of thermal stratification on air flow in city street canyons is minor. When the wind speed is small relative to the buoyancy force, the airflow in the street canyons is dependent on thermal stratification. When there is an adverse vertical temperature gradient, the greater the instability, the stronger the vertical mixing and the greater the flow rate caused by turbulence. The heat and pollutants can easily accumulate under stable atmospheric conditions when there is only a weak background wind or none at all.

1. Introduction

The impact of an urban heat island on energy consumption of buildings can be very significant. The accumulated heat in densely populated and compact modern cities can affect the surface energy balance as well as the energy consumption in a city. Reduced energy efficiency of air conditioning systems due to the urban heat island phenomenon has been a concern. Hassid et al. [1] showed that the urban heat island can increase the cooling energy and peak demand by as much as 100% in Athens. Even in London, the urban building cooling load can increase by 25%, according to a study by Watkins et al. [2], and for an optimized office in London, Kolokotroni et al. [3] showed that a rural site would only need 42% of the cooling required by an urban site due to the impact of the urban heat island on night ventilation strategies. Fung et al. [4] found that for a 1 °C urban ambient temperature rise, the annual electricity consumption in Hong Kong would increase by 9.2%, 3.0%, and 2.4% in domestic, commercial and industrial sectors, respectively. Lam et al. [5] also showed that the Hong Kong average annual cooling load in 2009–2100 would be 9.1% and 10.7% more than that in 1979–2008 for low and medium forcing, respectively; the percentage increase for energy use would be 4.3% and 4.9%, respectively. A number of possible causes are identified for urban heat islands, including increased absorption of solar radiation and anthropogenic heat generation, increased thermal storage, decreased evapotranspiration and reduced urban winds [6].

Here we focused on the study of thermal conditions and reduced urban winds in a high-rise compact city environment. Improving ventilation efficiency is a possible measure for improving energy efficiency in tropical high-rise compact cities like Hong Kong. In addition to heat removal, city ventilation is also important for removing air pollution [7]. Located along the southern coast of China, Hong Kong has a rugged terrain with hills rising steeply from the sea. Many complex thermally induced flows, such as natural convection flows on the vertical wall and mountain slope flows, land–sea breezes, mountain–valley winds, and urban heat island circulations, occur in Hong Kong [8]. Particularly on Hong Kong Island, most commercial/residential buildings are built on rugged terrain at different levels. The vertical natural convection wall flows and mountain slope flows become more important in such a high-rise city on days without wind. The interaction between these thermally induced flows may lead to a certain complexity of the Hong Kong urban boundary layer structure, which has a direct relationship with the transport and diffusion of urban heat and pollutants. Yang and Li [9] showed that the thermally induced air flows on the vertical wall and mountain slope surfaces can be significant under calm conditions. There have been a number of interesting studies on the urban heat island phenomenon in Hong Kong [10–13]. When studying urban thermal and ventilation conditions, atmospheric stability needs to be considered [14–17] and a large number of studies exist [18–20].

None of these studies quantified the amount of external air supplied to an urban environment, i.e. the city ventilation rate. City ventilation rate data are fundamental in estimating the urban heat balance and quantifying the ability of a city to remove heat and airborne pollutants. We therefore carried out this numerical study in

* Corresponding author. Tel.: +852 2219 4547; fax: +852 2858 5415.
E-mail address: lnyang08@gmail.com (L. Yang).

0378-7788/$ – see front matter © 2010 Elsevier B.V. All rights reserved.
doi:10.1016/j.enbuild.2010.06.005

Nomenclature

A	area [m^2]
ACH	air change per hour [h^{-1} or ACH]
H	building height [m]
k	kinetic energy of turbulence
L	domain width [m]
$\vec{n}$	normal direction of the street opening or street roof
p	pressure [Pa]
Pr	Prandtl number ($=\nu/\alpha$)
Pr_t	turbulent Prandtl number
q	ventilation flow rate [$m^3\,s^{-1}$]
R_{iB}	Bulk Richardson number ($=(g\beta\gamma)/(u_H/H)^2$)
Re	Reynolds number ($=uH/\nu$)
S	strain rate
T_0	reference temperature [°C]
T_b	building surface temperature [°C]
T_m	mountain surface temperature [°C]
T_s	sea temperature [°C]
u_i	velocity component [$m\,s^{-1}$]
$\bar{u}, \bar{v}, \bar{w}$	velocity components in x, y, z direction [$m\,s^{-1}$]
U	dimensionless velocity
V	volume [m^3]
W	domain length [m]
x, y, z	Cartesian coordinate

Greek symbols

α	thermal diffusivity [$m^2\,s^{-1}$]
α_T	inverse effective Prandtl number for energy equation
α_k	inverse effective Prandtl number for k equation
α_ε	inverse effective Prandtl number for ε equation
β	coefficient of thermal expansion [$°C^{-1}$]
γ	linear atmospheric vertical temperature gradient [°C/m]
κ	von Kármán constant (=0.4187)
μ	dynamic viscosity of air [$m^2\,s^{-1}$]
μ_{eff}	effective viscosity [$m^2\,s^{-1}$]
μ_{mol}	molecular viscosity [$m^2\,s^{-1}$]
μ_t	turbulence viscosity [$m^2\,s^{-1}$]
ε	dissipation rate of turbulence kinetic energy [$m^2\,s^{-3}$]
ρ	density of air [$kg\,m^{-3}$]
ν	kinematic viscosity [$m^2\,s^{-1}$]
ΔT	temperature difference [°C]

two simple Hong Kong models under different atmospheric conditions, attempting to gain an understanding of how city ventilation and thermal conditions can be affected by thermal stratification. Our numerical model was first validated using existing experimental data.

2. Methodologies

2.1. Model configuration

Most of Hong Kong's urban development is along the northern edge of Hong Kong Island and on the Kowloon peninsula. The Victoria harbor (see Fig. 1) lies in between. For simplicity, two basic Hong Kong city models are considered here (see Fig. 2). Efforts are made to capture the most essential urban wind flow features in the urban areas of Hong Kong, with a dominating easterly wind. Model I assumes there are no secondary streets, whereas Model II has secondary streets. We use a reduced scale model with a length

Fig. 1. 3D satellite image of Hong Kong (source: http://www.geocarto.com/new_hk.html).

scale ratio of 1/50 of the real size. The scaling parameters are summarized in Table 1. In this paper, only the model parameters are presented. The need for a small-scale model is due to the resolution requirements in modeling surface convection flows (slope flows and wall flows) (less than 1 mm) and the relatively large computational domain (8 km). The details of the computational geometry are shown in Table 2 and Fig. 3. The upstream length in front of the Kowloon buildings is about $5H$ and the downstream length is about $10H$ in the z direction (see Fig. 3c). In Hong Kong, the wind mostly channels through the Victoria Harbor and the easterly wind prevails throughout the year [21]. Therefore only the easterly wind is considered here. Thermal stratification effects are considered by assigning different temperatures to different levels for the incoming wind ($\gamma = 0.6$ °C/m, $\gamma = 0$ °C/m or $\gamma = -0.6$ °C/m).

2.2. Governing equations

As suggested by Cheng et al. [22], the k–ε Reynolds-averaged Navier–Stokes (RANS) turbulence models and the Reynolds stress turbulence model (RSM) can provide acceptable modeling approaches when compared to large eddy simulation (LES) methods, considering both solution accuracy and computational demands. The renormalization group (RNG) k–ε turbulence model proposed by Yakhot and Orszag [23] is chosen here to model the effect of turbulent flows, as recommended by various studies, e.g. [24]. In addition, the RNG k–ε model has been widely used for modeling the complex airflow within arrays of buildings or an urban area [25–27].

Using H (building height), u_H (reference velocity), and $\Delta T = \gamma H$ (vertical air temperature difference in the street canyon) as characteristic scales for length, velocity, and temperature, respectively, the non-dimensional steady-state governing equations are as follows:

Continuity equation

$$\frac{\partial U_i}{\partial X_i} = 0 \tag{1}$$

Momentum equation

$$\frac{\partial (U_i U_j)}{\partial X_j} = -\frac{\partial P}{\partial X_i} + \frac{1}{Re}\frac{\partial}{\partial X_j}\left[\frac{\nu_{eff}}{\nu}\left(\frac{\partial U_i}{\partial X_j} + \frac{\partial U_j}{\partial X_i}\right)\right] + \delta_{i3} Ri_B \theta \tag{2}$$

Energy equation

$$\frac{\partial (U_j \theta)}{\partial X_j} = \frac{1}{Re}\frac{\partial}{\partial X_j}\left(\frac{\alpha_T \nu_{eff}}{\nu}\frac{\partial \theta}{\partial X_j}\right) \tag{3}$$

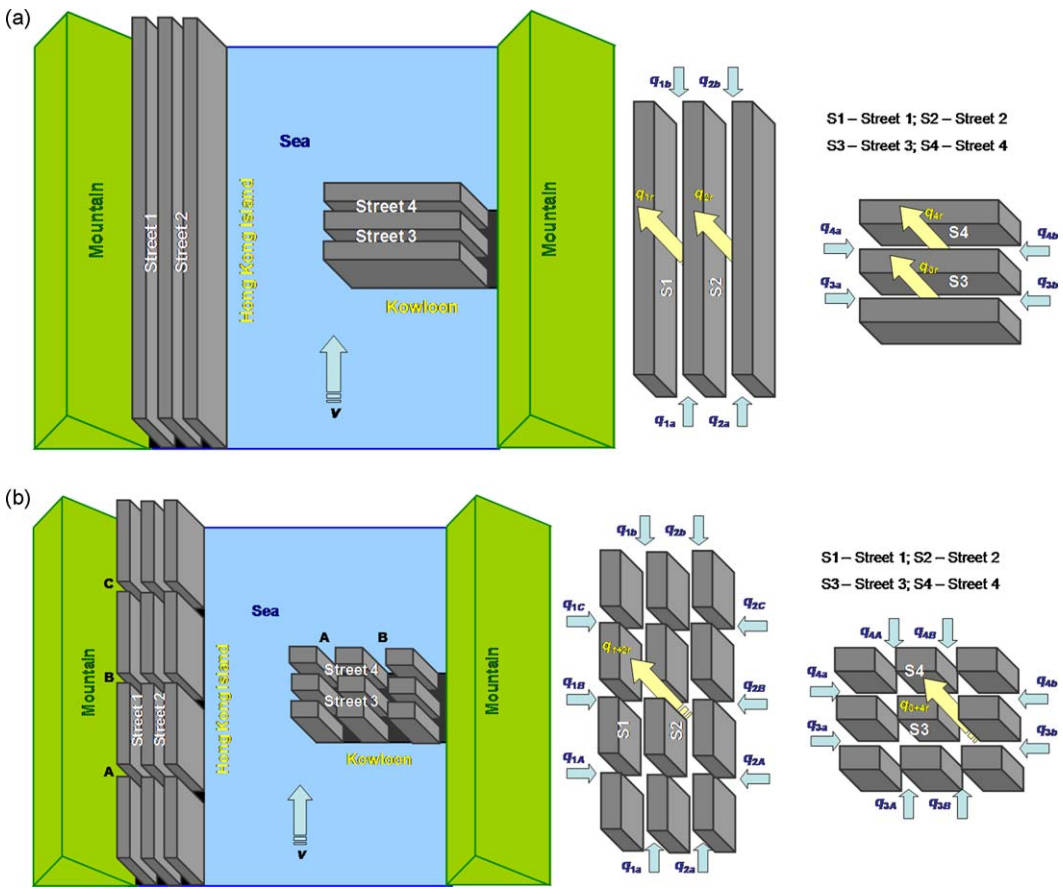

Fig. 2. Illustrations of simple small-scale Hong Kong city models and computational domain. (a) Model I and (b) Model II.

Table 1
The scaling parameters for the small-scale computational model and the modeled city.

Scaling parameters	Present model	Real city
Ambient vertical thermal gradient (°C/m)	$\gamma_m = \gamma$	$\gamma_r = \gamma_m/100$
Building height (m)	$H_m = H$	$H_r = 50H_m$
Wind velocity at the building height (m/s)	$u_m = u_H$	$u_r = 5u_m$
Building surface temperature (°C)	$T_m = T_b$	$T_r = T_m$
Bulk Richardson number	$Ri_m = Ri_B$	$Ri_r = Ri_m$
Ventilation flow rate (m^3/s)	$q_m = \int_A (\vec{u}\vec{i} + \vec{v}\vec{j} + \vec{w}\vec{k})\vec{n}dA$	$q_r = 1.25 \times 10^4 q_m$
Flow rate at roof level by turbulence (m^3/s)	$q_m = \int_A \frac{1}{2}\sigma_w dA$	$q_r = 1.25 \times 10^4 q_m$
ACH (h^{-1})	$ACH_m = 3600q_m/V$	$ACH_r = 0.1ACH_m$

Table 2
The geometrical parameters of the two simple small-scale Hong Kong models.

	Domain size: 80.32 m (L) × 76 m (W) × 30 m (H)				
Model I					
Mountain H_m	5 m	Mountain slope α	20°	Sea width L_s	9 m
Buildings A_1–A_3	76 m (L) × 0.2 m (W) × 2.5 m (H)			W_1, W_2	25 m, 50 m
Buildings E_1–E_3	5 m (L) × 0.2 m (W) × 2.5 m (H)			Street width	0.2 m
Volume S1 or S2	38 m^3			Volume S3 or S4	2.5 m^3
Model II					
Mountain H_m	5 m	Mountain slope α	20°	Sea width L_s	9 m
Buildings A_1–A_3	17.85 m (L) × 0.2 m (W) × 2.5 m (H)			W_1, W_2	25 m, 50 m
Buildings B_1–C_3	7.35 m (L) × 0.2 m (W) × 2.5 m (H)			Street width	0.2 m
Buildings D_1–D_3	42.85 m (L) × 0.2 m (W) × 2.5 m (H)			Buildings E_1–E_3	1.5 m (L) × 0.2 m (W) × 2.5 m (H)
Buildings F_1–F_3	1.6 m (L) × 0.2 m (W) × 2.5 m (H)			Buildings G_1–G_3	1.5 m (L) × 0.2 m (W) × 2.5 m (H)
Volume S1 + S2	76.9 m^3			Volume S3 + S4	5.6 m^3

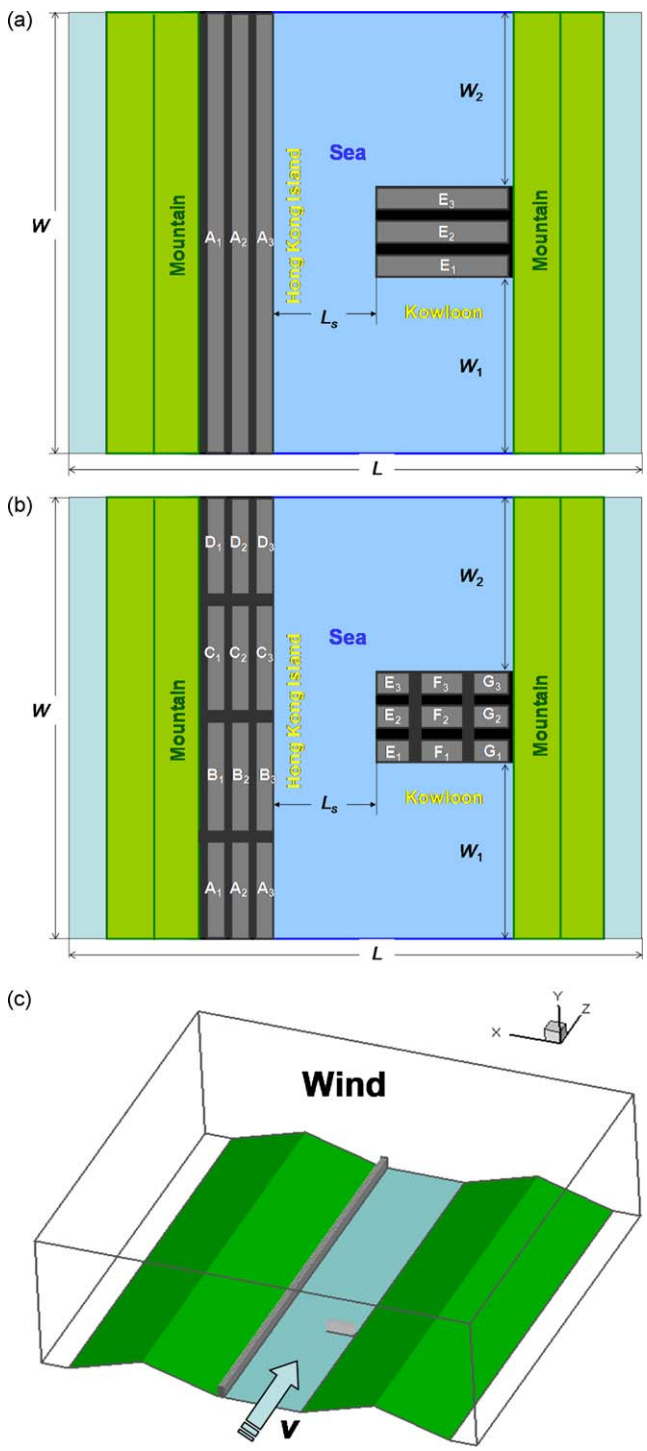

Fig. 3. Computational geometry of the small-scale Hong Kong city models. (a) Model I; (b) Model II; and (c) computational domain.

Turbulence kinetic energy

$$\frac{\partial(U_j K)}{\partial X_j} = \frac{1}{Re}\frac{\partial}{\partial X_j}\left(\frac{\alpha_k \nu_{eff}}{\nu}\frac{\partial K}{\partial X_j}\right) + C_\mu \frac{K^2}{\varepsilon}S^2 - \varepsilon \tag{4}$$

Dissipation rate of turbulence kinetic energy

$$\frac{\partial(U_j \varepsilon)}{\partial X_j} = \frac{1}{Re}\frac{\partial}{\partial X_j}\left(\frac{\alpha_\varepsilon \nu_{eff}}{\nu}\frac{\partial \varepsilon}{\partial x_j}\right) + \frac{\varepsilon}{K}(C_{1\varepsilon}C_\mu \frac{k^2}{\varepsilon}S^2 - C_{2\varepsilon}\varepsilon) - \frac{C_\mu \eta^3(1-\eta/\eta_0)}{1+\zeta\eta^3}\frac{\varepsilon^2}{K} \tag{5}$$

where the non-dimensional variables are as follows:

$$X_i = \frac{x_i}{H},\ U = \frac{u}{(u_H)},\ P = \frac{p}{\rho(u_H)^2},\ \theta = \frac{T-T_0}{\Delta T},\ K = \frac{k}{(u_H)^2},\ \varepsilon = \frac{\varepsilon H}{(u_H)^3}$$

The non-dimensional parameters are again the Reynolds number Re ($=u_H H/\nu$) and the Bulk Richardson number Ri_B ($=(g\beta(\partial T/\partial z))/(u_H/H)^2 = g\beta\gamma/(u_H/H)^2$). The effective turbulence kinetic viscosity [23], ν_{eff}, is calculated by:

$$\nu_{eff} = \nu_{mol}\left(1+\sqrt{\frac{\nu_t}{\nu_{mol}}}\right)^2 \tag{6}$$

where the turbulence kinetic viscosity $\nu_t = C_\mu(k^2/\varepsilon)$ and ν_{mol} is the molecular kinetic viscosity.

S is the modulus of the mean rate of strain tensor, S_{ij}, which is defined as:

$$S = \sqrt{2S_{ij}S_{ij}} \tag{7}$$

where $S_{ij} = \frac{1}{2}\left(\frac{\partial U_i}{\partial X_j} + \frac{\partial U_j}{\partial X_i}\right)$.

The coefficients α_T, α_k and α_ε are the inverse effective Prandtl number for energy, k and ε, respectively. They are computed using the following formula:

$$\left|\frac{\alpha-1.3929}{\alpha_0-1.3929}\right|^{0.6321}\left|\frac{\alpha+2.3929}{\alpha_0+2.3929}\right|^{0.3679} = \frac{\nu_{mol}}{\nu_{eff}} \tag{8}$$

where α_0 is equal to 1/Pr, 1.0 and 1.0, for the computation of α_T, α_k and α_ε, respectively. Another coefficient is $\eta = SK/\varepsilon$, and the model constants are $\eta_0 = 4.38$, $\zeta = 0.012$, $C_\mu = 0.0845$, $C_{1\varepsilon} = 1.42$ and $C_{2\varepsilon} = 1.68$.

2.3. Similarity considerations and model validation

The model's geometric and flow field similarities are taken into consideration. Strict similarity of atmospheric phenomena is generally not possible, but there is consensus on the basic non-dimensional parameters for modeling atmospheric processes of different scales [28–32]. Snyder [29,31] concluded from a literature review that the Rossby number may be ignored when modeling flows in a prototype with a length scale even greater than about 5 km in complex terrain. In addition, the Reynolds number, the Peclet number and the Reynolds–Schmidt product criteria may be disregarded if the model flow is of sufficiently high Reynolds number. The basic concept of the Reynolds number independence is that the main structure of the turbulence will be almost totally responsible for the bulk transfer of momentum and heat or mass if the flow is of sufficiently large Reynolds number [32]. Snyder [16] suggested a critical Reynolds number ($Re_H = u_H H/\nu$) of 4000. In the present study, the Reynolds numbers range from 8.2×10^4 to 2.5×10^5, which are sufficiently large. Hence we consider the similarity of the Richardson number with regard to atmospheric stability [17,18,32]. The bulk Richardson number Ri_B is used to quantify the ratio between the thermal effect and the inertial effect. However, there are very limited data regarding the Richardson number in urban areas. Based on some assumptions, typical Ri_B numbers (−0.03 to 0.17) for various stability conditions were calculated by Snyder [31]. Nakamura and Oke [18] found that street canyon air conditions remain unstable in summer in Japan (Ri_B: −3.73 to −0.08). Wakamatsu et al. [33] observed stable stratified conditions in winter in Sapporo. The bulk Richardson numbers

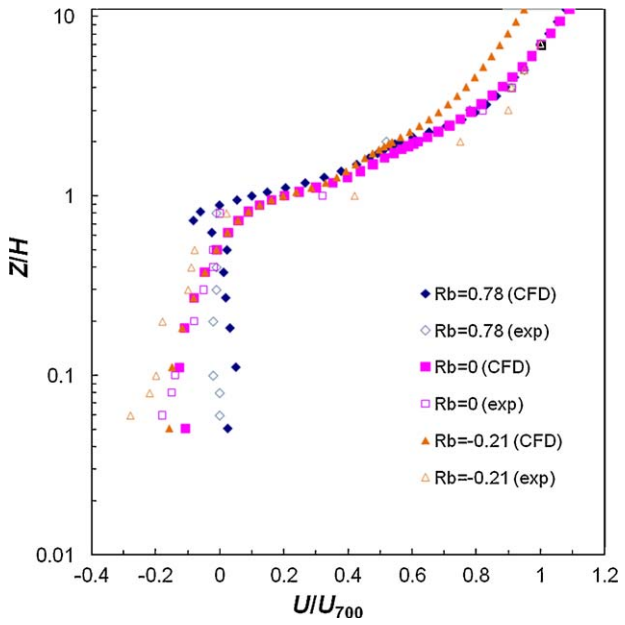

Fig. 4. U/U_{700} profiles at the central part of the street canyon ("exp": Uehara's wind tunnel experimental data [7]; "CFD": numerical study). R_b is the bulk Richardson number.

ranging from −0.5 to 0.5 in our study are chosen to be close to these field observation values.

The commercial CFD software Fluent 6.3.26 is used. The accuracy of the CFD model was evaluated using experimental data from the literature [17]. The test is on airflow in an urban street canyon with an aspect ratio of unity ($H/W = 1$) under different atmospheric conditions. The total number of grids in the 2D simulation is 23,210. Fig. 4 shows the simulated wind velocity profile in and above the street canyon, U/U_{700}, and measured data by Uehara et al. [17]. A good agreement can be found between the results shown in Fig. 4. The greater the instability, the higher the wind speed.

2.4. Numerical method

The velocity inlet boundary is used at the inlet with a power law formula $u(y) = u_H(y/H)^{0.143}$ (u_H: 0.5 and 1.5 m/s). The outflow boundary is defined at the domain outlet. The zero flux of all quantities is used at the top surface and two side surfaces. The no-slip condition is used at ground and building walls. Enhanced wall treatment in FLUENT, which combines a two-layer model with an enhanced wall function, is used as the wall model. According to the field measurements [9] and annual mean temperature data from Hong Kong Observatory, a constant temperature is specified for the mountain surface ($T_m = 15\,^\circ$C), building wall surface ($T_b = 30\,^\circ$C), harbor water surface ($T_s = 22\,^\circ$C) and the reference atmospheric air ($T_0 = 20\,^\circ$C) (see Fig. 3c). Using the second-order upwind scheme for the momentum equations and equations of turbulence kinetic energy, its dissipation rate and energy, Eqs. (1)–(5) are discretized using a finite volume method on a non-staggered grid [34]. The SIMPLE algorithm is used for the coupling between velocity and pressure. In both cases, the minimum mesh size near the wall and ground is 0.0008 m. The total number of grids is 532,968 for Model I and 1,049,031 for Model II.

2.5. Thermal and ventilation conditions

Thermal conditions in the urban space may be shown by plotting the air temperature distribution. Quantification of ventilation needs to be provided. An important concept about urban ventilation is introduced by Skote et al. [35] as follows. The airflow has a choice on the windward side of the urban canopy: flowing over the roof; flowing around the urban canopy; flowing into the street. The amount of air flowing into the street is very important for the dilution ability in the street cavity. When the wind dominates, the airflow may depend on the wind force, urban geometry and arrangement. When there is no wind, thermal buoyancy is the main force to drive air into the street canyon from the lateral openings and out through the street roof. The flow rate can be an important index for the effectiveness of the ventilation. The net volume flow rate at a plane is defined as:

$$q = \int_A (\bar{u}\vec{i} + \bar{v}\vec{j} + \bar{w}\vec{k})\vec{n}dA \tag{9}$$

where $\bar{u}$, $\bar{v}$ and $\bar{w}$ are the velocities in the x, y and z directions, respectively, and $\vec{n}$ is the normal direction of a plane.

The flow rate at roof level by turbulence is also important for ventilation:

$$q_{\text{turb}+} = q_{\text{turb}-} = \int_A \frac{1}{2}\sigma_w dA \tag{10}$$

where the fluctuation velocity $\sigma_\omega = (2k_r/3)^{1/2}$, and k_r is the turbulence kinetic energy at roof level.

The air change per hour (ACH) for an urban area can be:

$$\text{ACH} = \frac{3600 q_{\text{tot}}}{V} \tag{11}$$

where q_{tot} is the total flow rate for the street canyons considered (m^3/s), and V is the volume of street canyons (m^3).

3. Results and discussion

Two wind speeds (i.e. $u_H = 0.5$ and 1.5 m/s) are used to simulate both a thermal-buoyancy-dominated airflow ($Re = 8.2 \times 10^4$) and a wind-dominated airflow ($Re = 2.5 \times 10^5$) under three stratified atmospheric conditions (γ: −0.6, 0, 0.6 °C/m). The dominating force is seen by examining the resulting bulk Richardson number. For the second model with secondary streets (Model II), only a high wind speed (i.e. $u_H = 1.5$ m/s) is used to simulate wind-dominated flow under stable or unstable atmospheric conditions (γ: −0.6, 0, 0.6 °C/m), respectively.

Figs. 5 and 6 show the normalized temperature profile and streamlines along the street centerline for $Re = 8.2 \times 10^4$ ($u_H = 0.5$ m/s) and $Re = 2.5 \times 10^5$ ($u_H = 1.5$ m/s), respectively. The ventilation flow rates for each street are presented in Tables 3 and 4.

When the inflow is parallel to the street, the airflows in the street canyon are induced by the combined thermal buoyancy and wind forces. A higher surface temperature of the buildings and the ground than the surrounding air can produce upward airflows. The temperature difference can be height-dependent due to thermal stratification. The incoming winds can enhance or weaken the thermal-buoyancy-induced flows under different atmospheric conditions. When the inflow is perpendicular to the streets (S3 and S4), the upward-buoyancy flow in the street canyon can be blocked by the wind. The total ventilation flow rates and flow rates by turbulence for streets S3 and S4 are thus often smaller than those for streets S1 and S2 (see Tables 3 and 4), although the air change rate (ACH) for streets S3 and S4 is almost twice that for streets S1 and S2, due to a smaller void volume of S3 and S4.

The ventilation rates for streets S3 and S4 for the case of $Ri_B = -0.5$ (Table 3) are twice as large as that for $Ri_B = -0.06$ (Table 4). Hence the air temperature in the two streets is much lower for the former case than the latter (see Figs. 5 and 6).

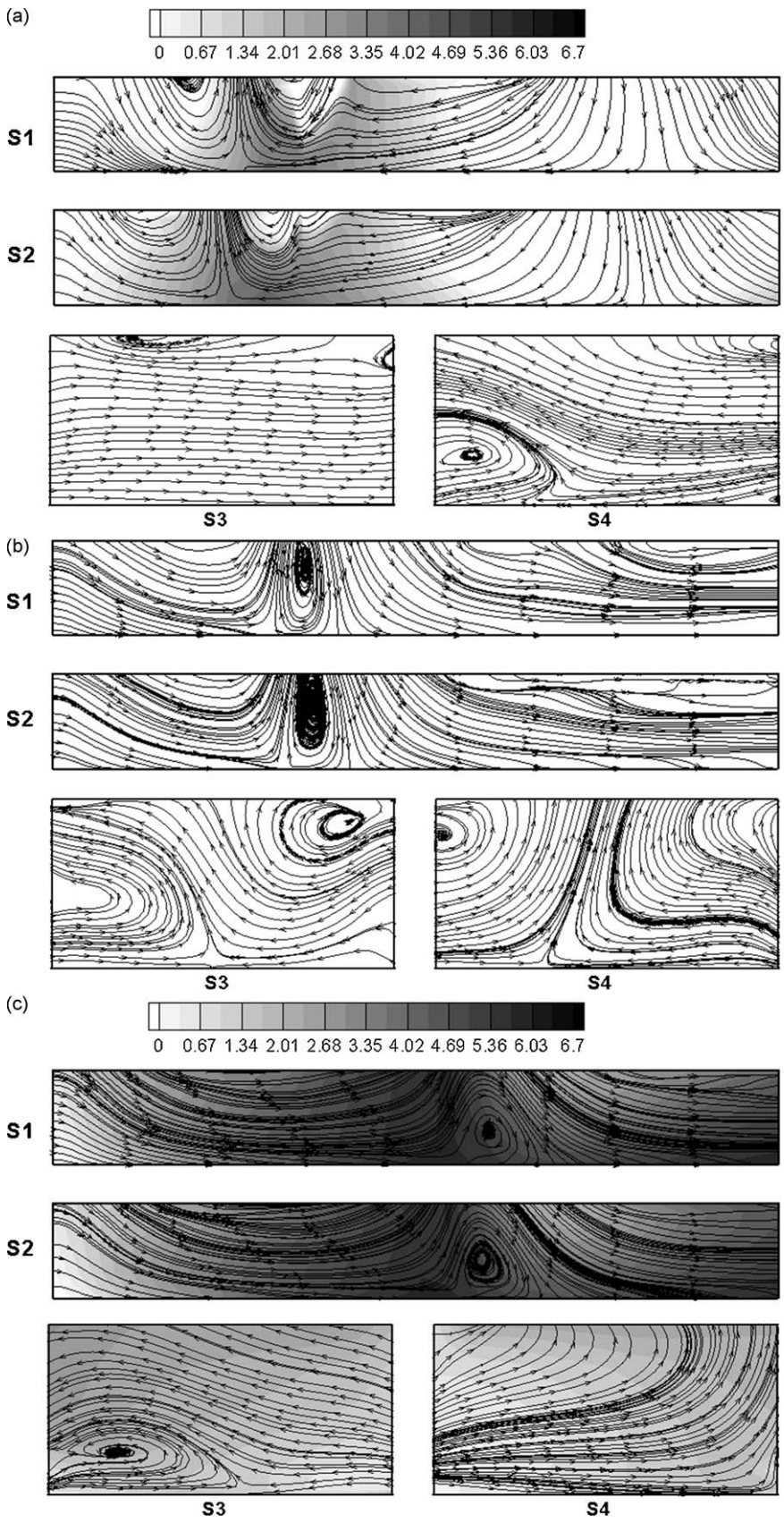

Fig. 5. The normalized temperature $(T - T_0)/|\gamma H|$ and streamlines along the centerline of streets S1–S4 for Re = 8.2×10^4 for Model I. (a) $Ri_B = -0.5$; (b) $Ri_B = 0$ (no temperature plot); (c) $Ri_B = 0.5$.

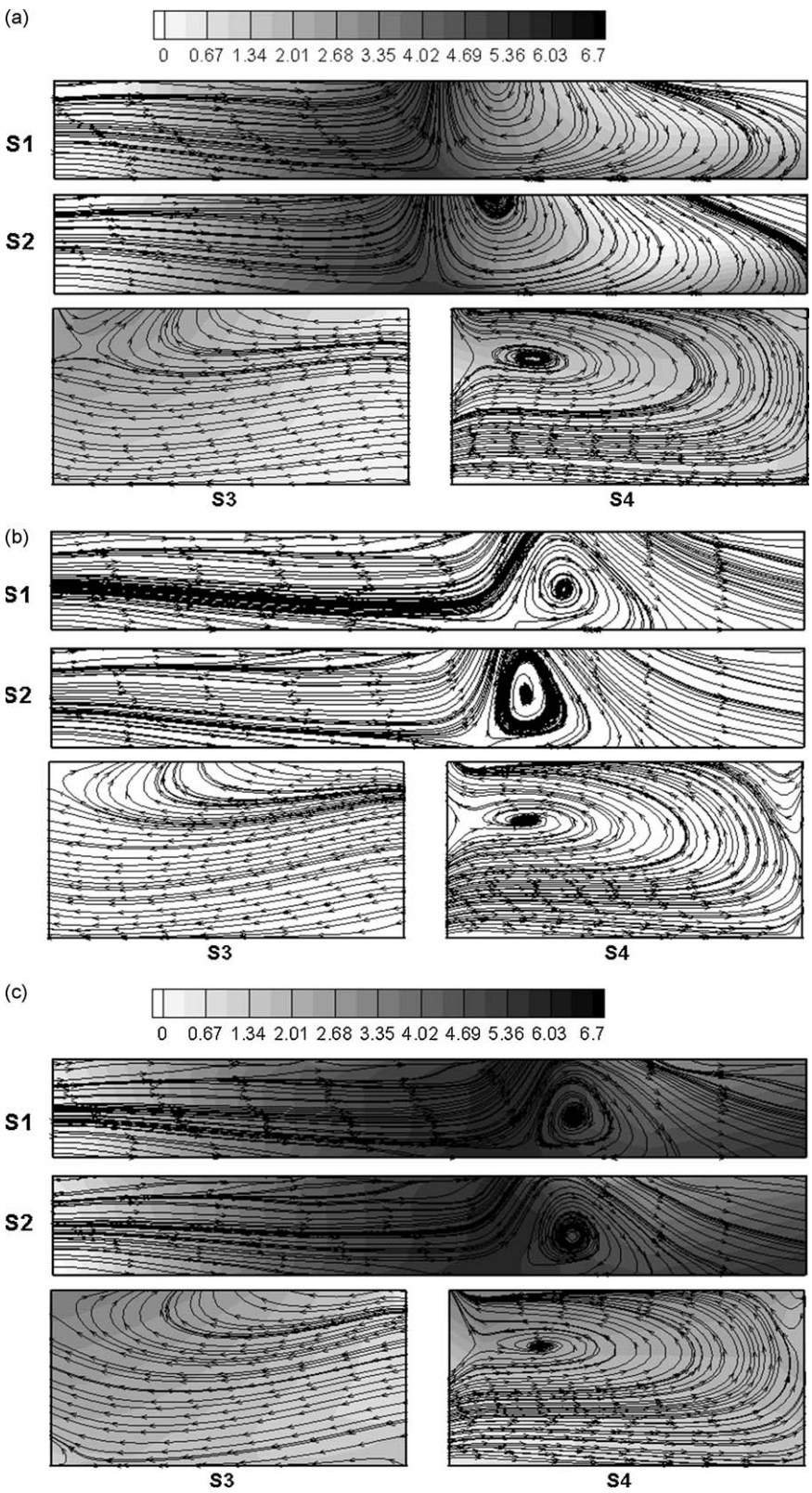

Fig. 6. The normalized temperature $(T - T_0)/|\gamma H|$ and streamlines along the centerline of streets S1–S4 for Re = 2.5×10^5 for Model I. (a) $Ri_B = -0.06$; (b) $Ri_B = 0$ (no temperature plot); (c) $Ri_B = 0.06$.

3.1. The effect of thermal buoyancy and wind

A higher wind speed (i.e. $u_H = 1.5$ m/s, Re = 2.5×10^5) means that the effect of wind is relatively larger than the thermal-buoyancy effect. Thermal buoyancy becomes more important and the rising thermal plume correspondingly increases when the wind speed is relatively small (i.e. $u_H = 0.5$ m/s, Re = 8.2×10^4). For Model I and the thermal-buoyancy-dominated case, the vertical mass exchange at the street roof level, i.e. the air entering and leaving through the roof, is much larger than the wind-dominated airflow (see

Table 3
Ventilation flow rates for Model I under different stratified conditions when thermal buoyancy dominates ($Re = 8.2 \times 10^4$) ("+" entering the street; "−" leaving the street; $q_{\#x}$: flow rate through opening #x where # = 1–4 and x = a, b, r: m^3/s; $q_{\#tot}$: ventilation rate of Street S# where # = 1–4: m^3/s; $q_{\#r\_turb}$: effective ventilation rate due to turbulence through the roof of Street S# where # = 1–4: m^3/s; ACH: h^{-1}).

Street S1					
Ri_B	q_{1a} (in/out)	q_{1b} (in/out)	q_{1r} (in/out)	q_{1tot} (ACH)	q_{1r_turb}
−0.5	0.22 (+0.22/0)	−0.19 (0/−0.19)	−0.03 (+1.26/−1.29)	1.48 (140.2)	0.68
0	0.22 (+0.22/0)	−0.26 (0/−0.26)	0.04 (+0.66/−0.62)	0.88 (83.4)	0.42
0.5	0.22 (+0.22/0)	−0.29 (0/−0.29)	0.07 (+0.99/−0.92)	1.21 (114.6)	0.55
Street S2					
Ri_B	q_{2a} (in/out)	q_{2b} (in/out)	q_{2r} (in/out)	q_{2tot} (ACH)	q_{2r_turb}
−0.5	0.22 (+0.22/0)	−0.21 (0/−0.21)	−0.01 (+1.23/−1.24)	1.45 (137.4)	0.84
0	0.22 (+0.22/0)	−0.19 (0/−0.19)	−0.03 (+0.67/−0.70)	0.89 (84.3)	0.48
0.5	0.22 (+0.22/0)	−0.36 (0/−0.36)	0.14 (+0.96/−0.82)	1.18 (111.8)	0.55
Street S3					
Ri_B	q_{3a} (in/out)	q_{3b} (in/out)	q_{3r} (in/out)	q_{3tot} (ACH)	q_{3r_turb}
−0.5	0.34 (+0.35/−0.01)	−0.26 (+0.02/−0.28)	−0.08 (+0.04/−0.12)	0.41 (590.4)	0.07
0	0.02 (+0.04/−0.02)	0.06 (+0.06/0)	−0.08 (+0.01/−0.09)	0.11 (158.4)	0.02
0.5	−0.03 (+0.03/−0.06)	0.14 (+0.14/0)	−0.11 (0/−0.11)	0.17 (244.8)	0.02
Street S4					
Ri_B	q_{4a} (in/out)	q_{4b} (in/out)	q_{4r} (in/out)	q_{4tot} (ACH)	q_{4r_turb}
−0.5	−0.08 (+0.05/−0.13)	0.27 (+0.28/−0.01)	−0.19 (0/−0.19)	0.33 (475.2)	0.03
0	0.07 (+0.08/−0.01)	0.09 (+0.09/0)	−0.16 (0/−0.16)	0.17 (244.8)	0.02
0.5	0.17(+0.19/−0.02)	−0.04 (0/−0.04)	−0.13 (0/−0.13)	0.19 (273.6)	0.03

Figs. 5 and 6). Because the background atmospheric conditions can have a significant impact on the upward airflow driven by thermal buoyancy, the airflow can be greatly influenced by thermal stratification when the background wind is relatively weak (see Fig. 5). When the wind effect becomes significant, the thermal stratification does not significantly affect the airflow and temperature distribution within the streets S1–S4 (see Fig. 6). As shown in Table 4, almost identical total flow rates can be found for the streets under different atmospheric conditions.

In comparison with the wind force, thermal buoyancy can also play an important role in street canyon ventilation by inducing comparable air flow rates for the streets, as seen by comparing q_{tot} in Tables 3 and 4. For streets S1 and S2, the total ventilation flow rate and the ACH increase with the increasing incoming wind

Table 4
Ventilation flow rates for Model I under different stratified conditions when wind dominates ($Re = 2.5 \times 10^5$) ("+" entering the street; "−" leaving the street; $q_{\#x}$: flow rate through opening #x where # = 1–4 and x = a, b, r: m^3/s; $q_{\#tot}$: ventilation rate of Street S# where # = 1,2,3,4: m^3/s; $q_{\#r\_turb}$ - effective ventilation rate due to turbulence through the roof of Street S# where # = 1–4: m^3/s; ACH: h^{-1}).

Street S1					
Ri_B	q_{1a} (in/out)	q_{1b} (in/out)	q_{1r} (in/out)	q_{1tot} (ACH)	q_{1r_turb}
−0.06	0.66 (+0.66/0)	−0.22 (0/−0.22)	−0.44 (+0.82/−1.26)	1.48 (140.2)	0.85
0	0.66 (+0.66/0)	−0.25 (0/−0.25)	−0.41 (+0.54/−0.95)	1.20 (113.7)	0.61
0.06	0.66 (+0.66/0)	−0.20 (0/−0.2)	−0.46 (+0.44/−0.90)	1.10 (104.2)	0.59
Street S2					
Ri_B	q_{2a} (in/out)	q_{2b} (in/out)	q_{2r} (in/out)	q_{2tot} (ACH)	q_{2r_turb}
−0.06	0.66 (+0.66/0)	−0.24 (0/−0.24)	−0.42 (+1.02/−1.44)	1.68 (159.2)	0.76
0	0.66 (+0.66/0)	−0.28 (0/−0.28)	−0.38 (+0.56/−0.94)	1.22 (115.6)	0.60
0.06	0.66 (+0.66/0)	−0.22 (0/−0.22)	−0.44 (+0.51/−0.95)	1.17 (110.8)	0.61
Street S3					
Ri_B	q_{3a} (in/out)	q_{3b} (in/out)	q_{3r} (in/out)	q_{3tot} (ACH)	q_{3r_turb}
−0.06	−0.10 (0/−0.10)	0.17 (+0.17/0)	−0.07 (+0.02/−0.09)	0.19 (273.6)	0.03
0	−0.11 (0/−0.11)	0.17 (+0.17/0)	−0.06 (+0.02/−0.08)	0.19 (273.6)	0.03
0.06	−0.10 (0/−0.10)	0.16 (+0.16/0)	−0.06 (+0.02/−0.08)	0.18 (259.2)	0.03
Street S4					
Ri_B	q_{4a} (in/out)	q_{4b} (in/out)	q_{4r} (in/out)	q_{4tot} (ACH)	q_{4r_turb}
−0.06	0.12 (+0.14/−0.02)	−0.02 (+0.01/−0.03)	−0.10 (0/−0.10)	0.15 (216.0)	0.03
0	0.10 (+0.12/−0.02)	0.00 (+0.02/−0.02)	−0.10 (0/−0.10)	0.14 (201.6)	0.03
0.06	0.12 (+0.13/−0.01)	−0.03 (+0.01/−0.04)	−0.09 (0/−0.09)	0.14 (201.6)	0.03

Table 5
Ventilation flow rates of streets S1-S4 for Model II under different stratified conditions when wind dominates ($Re = 2.5 \times 10^5$) ("+" entering the street; "−" leaving the street; $q_{\#r}$: flow rate through street roofs # where # = 1 + 2, 3 + 4: m^3/s; $q_{\#tot}$: ventilation rate of Streets S# where # = 1 + 2,3 + 4: m^3/s; $q_{\#r\_turb}$: effective ventilation rate due to turbulence through the street roofs # where # = 1 + 2, 3 + 4: m^3/s; ACH: h^{-1}).

Ri_B	Streets S1 + S2			Streets S3 + S4		
	q_{1+2r} (in/out)	q_{1+2tot} (ACH)	q_{1+2r_turb}	q_{3+4r} (in/out)	q_{3+4tot} (ACH)	q_{3+4r_turb}
−0.06	−1.58 (+1.24/−2.82)	3.25 (152.1)	1.29	−0.66 (0/−0.66)	1.62 (1041.4)	0.12
0	−1.28 (+1.09/−2.37)	2.86 (133.9)	1.23	−0.64 (0/−0.64)	1.59 (1022.1)	0.11
0.06	−1.20 (+1.00/−2.20)	2.71 (126.9)	1.11	−0.58 (0/−0.58)	1.49 (957.9)	0.10

when there is no thermal stratification (neutral case, $\gamma = 0\,^\circ C/m$) (see Tables 3 and 4). When there is a background temperature gradient ($\gamma = 6\,^\circ C/m$ or $\gamma = -6\,^\circ C/m$), the total air flow rates and ACH for the thermal-buoyancy-dominated case is much larger than the wind-dominated case. For streets S3–S4, the net ventilation flow rate through the roof of the streets decreases significantly when the incoming wind speed increases (see q_{3r}, q_{4r} in Tables 3 and 4). Relatively strong wind can greatly weaken the upward thermal-buoyancy flows.

3.2. The effect of thermal stratification

When wind speed is small and thermal buoyancy dominates the airflow (i.e. $u_H = 0.5$ m/s, $Re = 8.2 \times 10^4$), the temperature and velocity field are closely dependent on atmospheric conditions (see Fig. 5). Upward thermal buoyancy can be weakened when atmospheric conditions become stable. When the wind is parallel to streets S1–S2, the temperature in the street canyon increases with the increasing stratification stability (from unstable to stable atmospheric conditions). As shown in Table 3, both unstable and stable atmospheric conditions can lead to stronger vertical energy exchange. The greater the instability, the stronger the vertical mix in the street canyon. Thermal buoyancy can establish the upward flow and facilitate instability stratification. On the other hand, downward flow due to stable atmospheric conditions can penetrate into the street canyon through the street roof and weaken the upward flow by thermal buoyancy, which can form a more highly stable stratification in the street canyon. In this case, the heat will be kept in the street canyon (see Fig. 5).

As for streets S1–S2, the temperature in streets S3–S4 increases with increasing stratification stability (see Fig. 5). When the wind is perpendicular to streets S3–S4, the airflows in those streets are different under different atmospheric conditions. As shown in Fig. 5 and Table 3, the airflow through the left-hand side of street S3 (on the marine side) will change direction as atmospheric stratification becomes stronger. The opposite changes can be found on the right-hand side of street S3 (mountain side). Conversely, when stratification becomes stronger, the air entering street S4 from the mountain side to the marine side will change direction and enter from the marine side to the mountain side. The net airflow out of street S4 through the roof will decrease because the buoyancy effect is weakened by stable stratification (see Table 3).

When the wind dominates the airflow (i.e. $u_H = 1.5$ m/s, $Re = 2.5 \times 10^5$), thermal buoyancy is relatively weak. Thermal stratification does not impact the airflow within streets S1–S4 (see Fig. 6). As shown in Table 4, almost identical total flow rates can be found for the streets under different atmospheric conditions. In this case, the temperature distribution and airflow pattern in the street canyon are independent of atmospheric conditions (see Fig. 6).

3.3. The effect of secondary streets

In contrast to Model I, secondary streets are added in Model II. Only the results for a high wind speed (i.e. $u_H = 1.5$ m/s, $Re = 2.5 \times 10^5$) are reported here, to simulate the effect of thermal stratification and addition of secondary streets.

Table 5 shows the ventilation flow rates for streets S1–S2 and S3–S4, respectively. In general, the total ventilation flow rates and ACH for Model II increase significantly compared with those of Model I (see Tables 3–5). This is caused by the enhanced airflow through the additional secondary streets. In particular, the total ACH and flow rates by turbulence, q_{r_turb}, at roof level for streets S3–S4 in Model II are about four times and double of that of Model I, respectively.

The additional secondary streets can enhance airflow through the street canyon, but the enhancement also depends on the background atmospheric conditions. The greater the instability, the stronger the vertical mixing will be in the street canyon. The vertical airflow can directly influence the air flow rates into or out of the street canyon through the street openings. For streets S1–S2, a large amount of airflow can enter the streets through openings 1A–1C (mountain side) under unstable conditions (q: 0.1–0.18), which is nearly double that of the neutral case and triple that of the stable one. The airflows through the other side openings 2A–2C (marine side) do not change much as stratification changes. The airflows through the street roofs including inflow and outflow (q_r in Table 5) obviously decrease when the atmospheric conditions change from unstable to stable. Thus the total flow rate and the flow rate by turbulent fluctuation reduce with increasing stratification stability (see Table 5). For streets S3–S4, the airflow direction through the side openings (i.e. 3a, 4a and 4b, data not shown) varies when thermal stratification changes. As in streets S1–S2, the vertical mass exchange is dependent on thermal stratification. The greater the instability, the stronger the vertical mixing and the greater the flow rate by turbulent fluctuation (see Table 5).

Generally, the more air ventilation entering the streets, the greater will be the ability to remove heat and airborne pollutants by convection and turbulence for a dense urban city. Increasing the number of street openings can be more beneficial by introducing more airflow into and out of the street canyons. But airflow through the street openings and roof is also dependent on atmospheric conditions. Ventilation in street canyons can be reduced with increased stable atmospheric conditions.

4. Conclusions

Two simple small-scale models of Hong Kong were simulated using CFD to investigate the effects of thermal stratification on the city thermal conditions and ventilation by combined thermal buoyancy and winds.

For Model I, when the thermal-buoyancy force dominates, airflow is greatly influenced by atmospheric conditions. The greater the instability, the stronger the vertical mixing in the street canyon becomes. Stable atmospheric conditions can form downward flows into the street canyon and weaken the upward flow by thermal buoyancy, and thus form a more highly stable stratification in the street canyon. Heat and pollutants are shown to accumulate under stable atmospheric conditions when there is only a weak background wind or no wind at all. When the wind speed is relatively

large, the impact of thermal stratification on the airflow in the city street canyons is relatively minor. For Model II, the additional street openings can be more beneficial by introducing more airflow into and out of the street canyons. But it is also strongly dependent on atmospheric conditions. Ventilation in street canyons can be reduced with increased stable atmospheric conditions.

Acknowledgment

The work described in this paper was supported by a grant from the Research Grants Council of the Hong Kong Special Administrative Region, China (Project No. HKU 7145/07E).

References

[1] S. Hassid, M. Sanatamouris, N. Papanikolaou, A. Linardi, N. Klitsikas, C. Georgakis, D.N. Assimakopoulos, The effect of the Athens heat island on air conditioning load, Energy and Buildings 32 (2000) 131–141.
[2] R. Watkins, J. Palmer, M. Kolokotroni, P. Littlefair, The balance of the annual heating and cooling demand within the London urban heat island, BSER & T 23 (4) (2002) 207–213.
[3] M. Kolokotroni, I. Giannitsaris, R. Watkins, The effect of the London urban heat island on building summer cooling demand and night ventilation strategies, Solar Energy 80 (4) (2006) 383–392.
[4] W.Y. Fung, K.S. Lam, W.T. Hung, S.W. Pang, Y.L. Lee, Impact of urban temperature on energy consumption of Hong Kong, Energy 31 (2006) 2623–2637.
[5] J.C. Lam, K.K.W. Wan, T.N.T. Lam, S.L. Wong, An analysis of future building energy use in subtropical Hong Kong, Energy 35 (2010) 1482–1490.
[6] T.R. Oke, Boundary Layer Climates, 2nd ed., Routeledge, London, 1987.
[7] C.K. Chan, X. Yao, Air pollution in mega cities in China, Atmospheric Environment 42 (2008) 1–42.
[8] H. Tong, A. Walton, J. Sang, J.C.L. Chan, Numerical simulation of the urban boundary layer over the complex terrain of Hong Kong, Atmospheric Environment 39 (2005) 3549–3563.
[9] L. Yang, Y. Li, City ventilation of Hong Kong at no-wind conditions, Atmospheric Environment 43 (2009) 3111–3121.
[10] J.E. Nichol, An emissivity modulation method for spatial enhancement of thermal satellite images in urban heat island analysis, Photogrammetric Engineering & remote Sensing 75 (5) (2009) 547–556.
[11] W.Y. Fung, K.S. Lam, J. Nichol, S.W. Man, Derivation of nighttime urban air temperatures using a satellite thermal image, Journal of Applied Meteorology and Climatology 48 (4) (2009) 863–872.
[12] R. Giridharan, S.S.Y. Lau, S. Ganesan, Nocturnal heat island effect in urban residential developments of Hong Kong, Energy and Buildings 37 (9) (2005) 964–971.
[13] R. Giridharan, S. Ganesan, S.S.Y. Lau, Daytime urban heat island effect in high-rise and high-density residential developments in Hong Kong, Energy and Buildings 36 (6) (2004) 525–534.
[14] F. Pasquill, Atmospheric Diffusion: The Dispersion of Windborne Material from Industrial and Other Sources, D. Van Norstand Company Ltd., London, 1962.
[15] B.T. Yang, R.N. Meroney, Gaseous Dispersion into Stratified Building Wakes, 1970, AEC Rept. No. C00-2053-3.
[16] W.H. Snyder, Some observations of the influence of stratification on diffusion in building wakes, in: I.P. Castro, N.J. Rockliff (Eds.), Stably Stratified Flows and Dispersion over Topography, Claredon Press, Oxford, England, 1994, pp. 301–324.
[17] K. Uehara, S. Murakami, S. Oikawa, S. Wakamatsu, Wind tunnel experiments on how thermal stratification affects flow in and above urban street canyons, Atmospheric Environment 34 (2000) 1553–1562.
[18] Y. Nakamura, T.R. Oke, Wind, temperature, and stability conditions in east–west oriented urban canyon, Atmospheric Environment 22 (1988) 2691–2700.
[19] Y. Ogawa, P.G. Diosey, Surface roughness and thermal stratification effects on the flow behind a two-dimensional fence—I. Field study, Atmospheric Environment 14 (1980) 1301–1308.
[20] Y. Ogawa, P.G. Diosey, Surface roughness and thermal stratification effects on the flow behind a two-dimensional fence—II. A wind tunnel study and similarity considerations, Atmospheric Environment 14 (1980) 1309–1320.
[21] F.W.H. Yik, T.Y. Lo, J. Burnett, Wind data for natural ventilation design in Hong Kong, Building Services Engineering Research and Technology 24 (2003) 125–136.
[22] Y. Cheng, F.S. Lien, E. Yee, R. Sinclair, A comparison of large eddy simulations with a standard k–ε Reynolds-averaged Navier–Stokes model for the prediction of a fully developed turbulent flow over a matrix of cubes, Journal of Wind Engineering and Industrial Aerodynamics 91 (11) (2003) 1301–1328.
[23] V. Yakhot, S.A. Orszag, Renormalization group methods in turbulence, Journal of Scientific Computing 1 (1986) 1–51.
[24] J.-J. Kim, J.-J. Baik, A numerical study of the effects of ambient wind direction on flow and dispersion in urban street canyons using the RNG k–ε turbulence model, Atmospheric Environment 38 (2004) 3039–3048.
[25] X. Xie, C.-H. Liu, D.Y.C. Leung, M.K.H. Leung, Characteristics of air exchange in a street canyon with ground heating, Atmospheric Environment 40 (2006) 6396–6409.
[26] X. Xie, C.-H. Liu, D.Y.C. Leung, Impact of building facades and ground heating on wind flow and pollutant transport in street canyons, Atmospheric Environment 41 (2007) 9030–9049.
[27] J. Hang, M. Sandberg, Y. Li, Effect of urban morphology on wind condition in idealized city models, Atmospheric Environment 43 (4) (2008) 869–878.
[28] J.E. Cermak, V.A. Sandborn, E.J. Plate, G.H. Binder, H. Chuang, R.N. Meroney, S. Ito, Simulation of Atmospheric Motion by Wind Tunnel Flows, Fluid Dyn. and Diff. Lab. Rpt. No. CER66JEC-VAS-EJP-GJB-HC-RNM-S117, Colo. State Univ., Ft. Collins, CO, 1966, p. 102.
[29] W.H. Snyder, Similarity criteria for the application of fluid models to the study of air pollution meteorology, Boundary-Layer Meteorology 3 (1972) 113–134.
[30] W.H. Snyder, The EPA Meteorological Wind Tunnel—Its Design, Construction and Operating Characteristics, Publication No. EPA-600/4-79-051, Environmental Protection Agency, Research Triangle Park, USA, 1979, pp. 1–63.
[31] W.H. Snyder, Guidelines for fluid modelling of atmospheric diffusion, Publication No. 600/8-81-009, Environmental Protection Agency, Research Triangle Park, USA, 1981, pp. 3–42.
[32] W.H. Snyder, Fluid modelling of pollutant transport and diffusion in stably stratified flows over complex terrain, Annual Review of Fluid Mechanics 17 (1985) 239–266.
[33] S. Wakamatsu, I. Uno, A. Nakamura, Research on dispersion phenomena on an urban scale, in: Y. Matsuso (Ed.), Ministry of Education Special Report on "Environmental Sciences" Research, 1986, pp. B-296, R15-1, 5-104.
[34] S.V. Patankar, Numerical Heat Transfer and Fluid Flow, McGraw-Hill, New York, 1980.
[35] M. Skote, M. Sandberg, U. Westerberg, Numerical and experimental studies of wind environment in an urban morphology, Atmospheric Environment 39 (2005) 6147–6158.